processes

MDPI

Article

Valorization of *Inga feuilleei* (Pacay) Seeds as a Promising Adsorbent for the Removal of Direct Red 80 Dye in Aqueous Solution—Kinetics, Isotherms, Thermodynamics, and Techno-Economic Analysis

Elvis G. Gonzales-Condori [1,*], Madelin L. Sotomayor-Asencio [1], Marycielo F. Mayhuire-Centeno [1], Olivia A. Paz-Corrales [1], Jonathan Gonzales-Condori [2] and José A. Villanueva-Salas [2]

[1] Grupo de Investigación en Biotecnología y Ciencia de los Alimentos, Universidad Tecnológica del Perú, Arequipa 04001, Peru
[2] Escuela de postgrado, Universidad Católica de Santa María (UCSM), Urb. San José s/n Umacollo, Arequipa 04002, Peru
* Correspondence: elvgonzalesc@gmail.com

Abstract

Textile wastewater pollution is a global issue that requires attention due to its potential negative environmental impacts. Therefore, in the present investigation, *Inga feuilleei* seed (IFS) powder was used as a potential adsorbent of Direct Red 80 (DR80) dye in synthetic water. The results showed that the highest removal efficiency was achieved at pH = 2 and an IFS powder particle size of 150 µm. ART-FTIR analysis of IFS dust showed the presence of -OH, C=C, and C-H groups. The kinetic study revealed a better fit of the experimental adsorption data to the pseudo-second-order kinetics, suggesting that the mechanism governing the adsorption process is chemisorption. The maximum adsorption capacity of DR80 on IFS powder was 133.11, 146.78, 152.78, and 183.51 mg/g at 20, 30, 40, and 50 °C, respectively. According to the thermodynamic study, the process is endothermic and spontaneous. Finally, the use of IFS powder is a cost-effective alternative since the project approach for the development of the production process of this adsorbent is feasible and profitable. In conclusion, IFS powder is a cost-effective adsorbent for removing DR80 in water, and the process could be scaled up in removal studies on textile wastewater.

Keywords: seeds; *Inga feuilleei*; adsorption; techno-economic analysis; Direct Red 80; water

Check for updates

Academic Editors: Dragana D. Vasić Anićijević, Miloš D. Milović and Marija Ječmenica Dučić

Received: 25 January 2026
Revised: 3 March 2026
Accepted: 6 March 2026
Published: 18 March 2026

Copyright: © 2026 by the authors. Licensee MDPI, Basel, Switzerland. This article is an open access article distributed under the terms and conditions of the Creative Commons Attribution (CC BY) license.

1. Introduction

Industrial activity has triggered environmental problems due to the release of wastewater contaminated with different emerging pollutants such as pharmaceuticals, cosmetics, pesticides, microplastics, heavy metals, and textile dyes [1]. In particular, textile wastewater is characterized by color and other substances that have made the treatment of these effluents a challenge [2]. Their high chemical and biochemical demand for oxygen and their color reduce the photosynthesis of aquatic plants, thus inhibiting their growth or bioaccumulating in these plants, which could represent risks of toxicity in aquatic living beings; in addition to this, these factors also harm the aesthetics of water bodies [3]. It is also known that these textile dyes can biomagnify and be transferred in the food chain and can be a risk to human health due to their possible carcinogenic and mutagenic effects [4]. There are different types of synthetic dyes, such as azo dyes, which, when in contact with

human intestinal microflora, skin microflora, and microorganisms in the environment, can cause the reduction of azo groups, giving rise to products such as benzidine, which is associated with tumor formation, and p-phenylenediamine, which is an allergen. Aromatic amines may also be associated with diseases, including cancer [5]. One of the most widely studied azo dyes is Direct Red 80 (DR80) ($C_{45}H_{32}N_{10}O_{21}S_6.6Na$), which can cause skin irritation and eye irritation and may be toxic to aquatic organisms [6]. For this reason, this dye must be removed before it reaches the environment using efficient technologies; the use and production of DR80 is increasing, generating a large amount of wastewater that is discharged into the environment without treatment [7].

Since the 1950s, efforts have been made to develop technologies that focus on the removal of these dyes from wastewater by physical processes such as ultrafiltration, electrocoagulation, electrochemical combustion, and radiation; chemical processes such as ozonation and the Fenton reaction; and some biological processes, such as the use of microorganisms and phytoremediation, which have also been developed [8]. However, the difficulty of their application has led to the proposal of more alternatives to more efficiently remove dyes from wastewater [9,10]. Different alternatives have been developed for the removal of DR80, including electrocoagulation [11], adsorption [12,13], photocatalysis [14,15], Fenton process [16], and membrane-based technologies [17–22].

On the other hand, in recent years, emphasis has been placed on the use of technologies that are not only effective but also reliable, sustainable, and cost-effective for scaling to real environments [23]. Among the cost-effective processes is adsorption, which is mainly based on chemical and physical adsorption [24]. Thus, adsorption processes are ideal in environmentally friendly and low-cost technologies [25]. However, most studies focus on demonstrating the capacity of agro-industrial waste to remove pollutants [26], but they do not allow the projection of its potential scaling to real environments, which limits its application. For this reason, in the present research, a techno-economic analysis was developed to approximate the incorporation of this technology into real world environments.

The genus *Inga* is present in South and Central America and comprises more than 300 species, generally composed of husks and seeds surrounded by edible pulp; the main waste after consumption is the seeds and husk [27]. The residues of different species of the genus Inga have proven to be useful for removing contaminants from aqueous media, such as the case of *Inga edulis* bark that removes Cr (VI) [28] and polyphenols [29]; likewise, *Inga laurina* removes methylene blue [30], *Inga marginata* removes gentian violet [31], and *Inga nobilis* removes of 14.81% of the color of real raw water [32].

The species *Inga feuilleei* was domesticated in Peru during the Inca Empire and spread to countries such as Chile, Bolivia, and Ecuador [33]. This species was introduced in other places such as Australia and Malaysia [34]. Of the fruit of *Inga feuilleei*, approximately 8.54% corresponds to the seed, 11.47% to the peels, and 61.12% to the pulp. Therefore, in the present investigation, *Inga feuilleei* seeds were used as a potential adsorbent of Direct Red 80 from aqueous solutions; for this purpose (1) the adsorbent was characterized before and after the adsorption process, (2) the effect of particle size and pH on the adsorption process was evaluated, (3) the kinetic, isothermal and thermodynamic parameters of the adsorption process were evaluated, and (4) a techno-economic analysis was carried out to evaluate the possible implementation of a plant for the production of the adsorbent.

2. Materials and Methods

2.1. Reagents

Direct Red 80 dye was obtained from Sigma Aldrich. Hydrochloric acid, sodium hydroxide, and sodium chloride were obtained from Merck.

2.2. Quantification of Direct Red 80 in Water

Direct Red 80 (DR80) quantification was performed on the Genesys 150 UV/VIS spectrophotometer, Thermo Fisher Scientific (Waltham, MA, USA). The method consisted of preparing a calibration graph using DR80 calibration solutions from 1 to 50 mg/L. These solutions were analyzed at 530 nm, obtaining a coefficient of determination $R^2 = 0.9995$. Also, the equation of the line $y = 0.02943x + 0.0041$ was obtained and used for the quantification of DR80 in the treated water, where "x" is the concentration of DR80 in mg/L and "y" is the absorbance at 530 nm.

2.3. Adsorption Process

Figure 1 shows the adsorption process of Direct Red 80 (DR80) on *Inga feuilleei* seed (IFS) powder. The procedure began by obtaining IFS from organic waste produced at the "Mi Mercado" shopping center in the Andrés Avelino Cáceres Metropolitan Market in the district of José Luis Bustamante y Rivero in the province and department of Arequipa, Peru (−16.4234231, −71.5365881). The IFS, previously washed and dried at room temperature (7 days), was pulverized in a blade mill. Subsequently, the IFS powder, previously dried at 40 °C for 24 h, was sorted into four particle size fractions using 150, 300, 425, and 600 µm mesh to perform adsorption experiments with each particle size. For the adsorption studies at controlled temperature, a glass beaker with a jacket was used, where a synthetic solution of DR80 was placed at a determined concentration and an adsorbent dosage (IFS powder) of 1 g/L, and an agitation speed of 350 rpm for 240 min. The pH of the medium was adjusted using 0.1 M HCl and 0.1 M NaOH. At the end of the time, 5 mL samples were collected into centrifuge tubes and centrifuged at 4000 rpm for 10 min. The supernatant was analyzed spectrophotometrically to determine its absorbance at 530 nm and subsequently calculate the concentration of DR80. The initial concentration "C_0" and the final concentration "C_f" of DR80 in mg/L were determined, and then the removal efficiency (removal (%)) was calculated using Equation (1). All adsorption experiments were performed in triplicate.

$$\text{Removal } (\%) = \frac{(C_0 - C_f)}{C_0} \times 100 \quad (1)$$

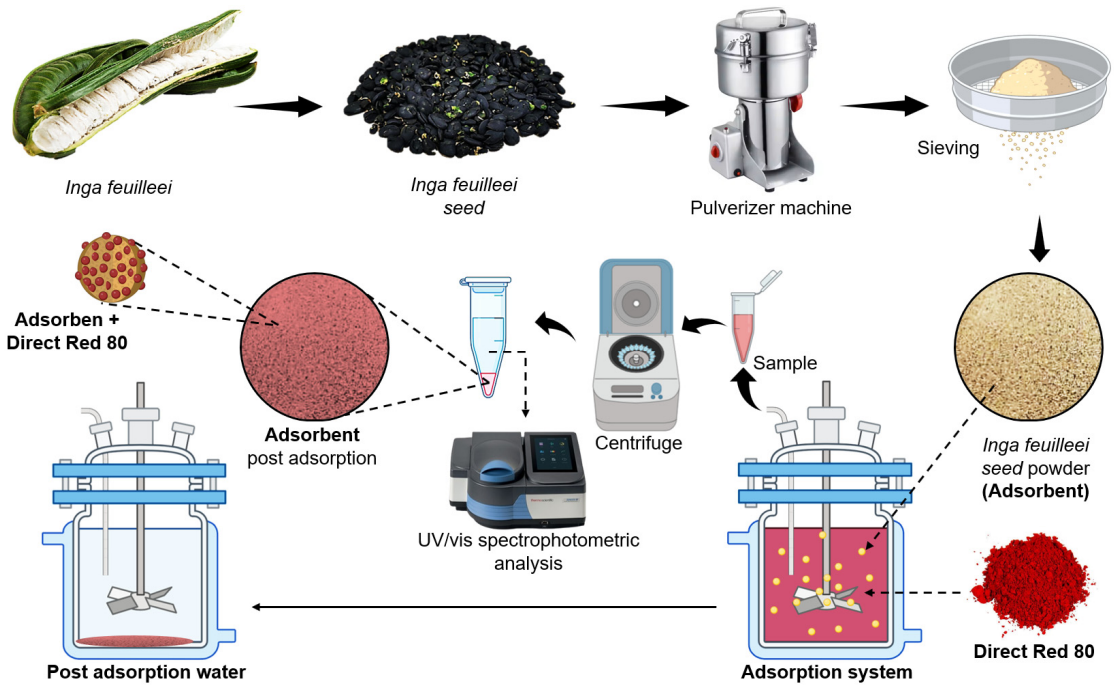


Figure 1. Adsorption process of Direct Red 80 onto *Inga feuilleei* seed powder.

2.4. Characterization

First, characterization by scanning electron microscopy was conducted on the Scanning Electron Microscope Scios 2 DualBeam (Thermo Fisher Scientific, Waltham, MA, USA) to evaluate the morphology of the IFS powder. Secondly, the IFS powder was characterized by Attenuated Total Reflectance—Fourier Transform Infrared Spectroscopy (ATR-FTIR) on Cary 630 of Agilent (Santa Clara, CA, USA) to identify the functional groups present on the IFS powder.

Third, the point of zero charge (pH_{PZC}) was determined using the methodology developed by Gonzales-Condori et al. [35] with some modifications. The procedure consisted of weighing 50 mg of IFS powder into 100 mL flasks, where 50 mL of a 0.1 M NaCl solution was added, with the pH previously adjusted to initial pH values "pH_i" of 2 to 11 using 0.1 M HCl and 0.1 M NaOH. Then, agitation was started for 24 h at 150 rpm. At the end of the time, the final pH "pH_f" was measured. Subsequently, ΔpH (pHf–pHi) was calculated, and pH_i versus ΔpH was plotted.

2.5. Particle Size Effect on the Removal Process

Adsorption experiments were conducted to select the particle size that achieves the highest removal efficiency. For this, particle sizes of 150, 300, 425, and 600 µm were used at a dosage of 1 g/L each using an initial DR80 concentration of 100 mg/L at 20 °C and pH = 4. At the end of the experiments, the removal efficiency was calculated. With triplicate results, a one-way analysis of variance (ANOVA) and Tukey's test were performed to determine the optimal particle size for the following experiments.

2.6. pH Effect on the Removal Process

Once the particle size with the highest removal efficiency was selected, adsorption experiments were conducted using an IFS powder dosage of 1 g/L, an initial concentration of 100 mg/L at 20 °C. At the end of the experiments, the removal efficiency was calculated. With triplicate results, ANOVA and Tukey's test were performed to determine the optimal pH for the following experiments.

2.7. Kinetics

Using a particle size and pH of the highest removal efficiency, experiments were conducted to evaluate the adsorption kinetics using a dosage of 1 g/L IFS powder for 240 min. Experiments were conducted at initial concentrations of 100, 200, 300, and 400 mg/L of DR80, and at temperatures of 20, 30, 40, and 50 °C. Samples of 5 mL were taken in centrifuge tubes at times 0, 5, 10, 30, 60, 90, 120, 180, and 240 min to quantify the concentration of DR80 and calculate the adsorption capacity "q_t" in mg/g using Equation (2) [36].

$$q_t = \frac{C_i - C_f}{m} \times V \tag{2}$$

where "m" is the weight of IFS powder in g and "V" corresponds to the volume of DR80 solution in L.

Subsequently, the kinetic study was performed taking into account the pseudo-first order using Equation (3) and the pseudo-second order using Equation (4) [36].

$$q_t = q_e(1 - e^{-k_1 t}) \tag{3}$$

$$q_t = \frac{k_2 q_e^2 t}{1 + k_2 q_e t} \tag{4}$$

where "k_1" corresponds to the pseudo-first-order constant (min^{-1}), and "k_2" is the pseudo-second-order constant (g $mg^{-1}min^{-1}$). On the other hand, "q_e" is the adsorption capacity at equilibrium. To calculate these parameters, "t" versus "q_t" was plotted.

2.8. Adsorption Isotherms

Adsorption isotherms were evaluated at 20, 30, 40, and 50 °C, using experiments at initial concentrations of 100, 200, 300, and 400 mg/L DR80. The models used were the Langmuir and Freundlich nonlinear models, as given by Equations (5) and (6), respectively.

$$q_e = \frac{q_m K_L C_e}{1 + K_L C_e} \tag{5}$$

$$q_e = K_f {C_e}^{1/n} \tag{6}$$

where "C_e" corresponds to the concentration of DR80 in mg/L at equilibrium, and "q_m" corresponds to the maximum adsorption capacity in mg/g of IFS powder. "K_L" corresponds to the Langmuir constant (L/mg), and "n" corresponds to the Freundlich constant [37].

2.9. Thermodynamic Study

The thermodynamic parameters were calculated. The entropy (ΔS^0), enthalpy (ΔH^0), and Gibbs energy (ΔG^0) were determined with the following equations (Equations (7)–(10)) [37].

$$\Delta G^0 = \Delta H^0 - T\Delta S^0 \tag{7}$$

$$\Delta G^0 = -RT \ln k_c \tag{8}$$

$$k_c = \frac{q_e}{C_e} \tag{9}$$

$$\ln Kc = -\frac{\Delta H^0}{RT} + \frac{\Delta S^0}{R} \tag{10}$$

where "T", "R", and "K_c" correspond to the temperature (K), the universal gas constant (J/mol·K), and the equilibrium constant (L/g), respectively.

2.10. Evaluation of Adsorbent Reuse

The efficiency of DR80 removal using IFS powder was evaluated in five cycles. The DR80 adsorbed onto the IFS powder was desorbed. The IFS powder with the adsorbed DR80 was dried in an oven until dry, and then the IFS + DR80 powder was transferred to beakers where desorption was carried out using distilled water adjusted to pH = 12 with 1 M NaOH. Agitation was carried out for 120 min, after which the IFS powder was recovered and placed in an oven at 40 °C until dry. The IFS powder was reused for the second adsorption cycle. The same procedure was followed for the third, fourth, and fifth cycles. All experiments were performed in triplicate. Finally, the removal efficiencies for each cycle were calculated.

2.11. Techno-Economic Analysis Process

The techno-economic analysis was developed taking into account a previous study [37], to implement a plant for the production of IFS powder as an alternative for the treatment of water contaminated with DR80. This analysis was carried out to evaluate the possible feasibility and profitability. Taking into account the above, the profitability indexes were calculated, which correspond to the Net Present Value "NPV", the Internal Rate of return

'IRR', the benefit/cost "B/C", and the Investment Recovery Period "IRP" using Equations (11), (12), (13), and (14), respectively.

$$VAN = \left(\frac{CF_1}{(1+i)} + \frac{CF_2}{(1+i)^2} + \frac{CF_3}{(1+i)^3} + \frac{CF_n}{(1+i)^n} \right) - I_0 \quad (11)$$

$$IRR - I_0 \left(\frac{CF_1}{(1+i)} + \frac{CF_2}{(1+i)^2} + \frac{CF_3}{(1+i)^3} + \frac{CF_n}{(1+i)^n} \right) = 0 \quad (12)$$

$$\frac{B}{C} = \frac{Updated\ benefits - Updated\ \cos\ ts}{Initial\ investment} \quad (13)$$

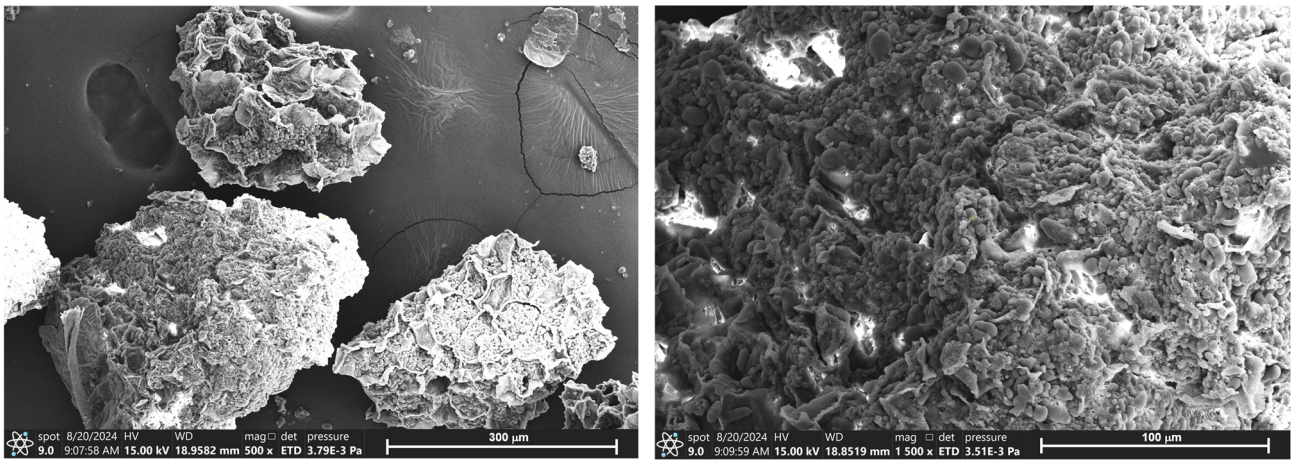
$$IRP = A + \frac{B' - C'}{D} \quad (14)$$

where "CF_n" is the Cash Flow for each year "n". "I_0" is the initial investment, and "i" is the discount rate. "A" is the immediate previous year of recovery, "B'" is the initial investment, "C'" is the accumulated cash flow of the year before recovery, and finally "D" is the economic cash flow of the year where the investment is recovered. In the Supplementary Material, the calculations of each variable are presented step by step. A positive *NPV* value indicates that the project is viable, and the *B/C* value is greater than 1, and an *IRP* value greater than the Cost of Opportunity of Capital (*COK*, Data in Supplementary Material) indicates profitability [37].

3. Results and Discussion

3.1. SEM Characterization

Figure 2 shows SEM micrographs of *Inga feuilleei* seed powder (IFS) at 500× (Figure 2a) and 1500× (Figure 2b). It is observed that the IFS powder presents a rough, irregular, and heterogeneous structure, with the presence of pores. These structures are characteristic of lignocellulosic structures [38] and have high fiber content [39]. Similarly, in another study, they found heterogeneous structures with larger pore sizes [40].



(**a**) (**b**)

Figure 2. SEM analysis of *Inga feuilleei* seed powder at (**a**) 500× and (**b**) 1500×.

3.2. Point of Zero Charge

Figure 3 shows the point of zero charge (pH_{PZC}) analysis of the IFS powder. It is observed that pH_{PZC} = 4.67, which indicates that at pH = 4.67 the charge on the IFS surface is zero; at pH< 4.67 it would be positively charged, and at pH > 4.67 it would be negatively charged. This would influence the efficiency of adsorption processes, since at

pH< pH_{PZC} protonation of the adsorbent surface favors adsorption of negatively charged substances [41].

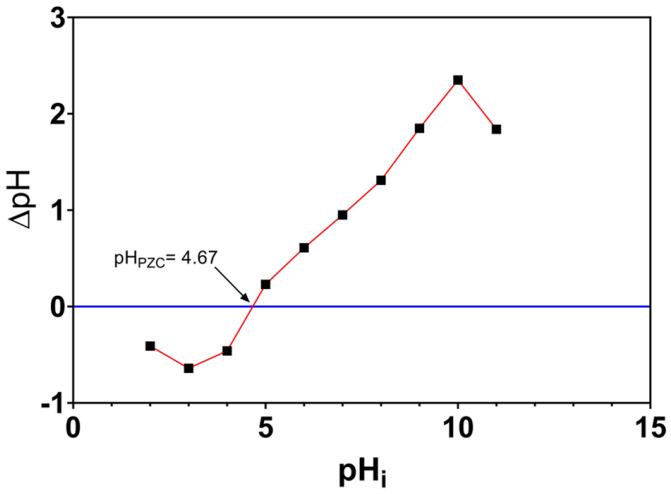


Figure 3. Point of zero charge of *Inga feuilleei* seed powder.

3.3. Effect of the Particle Size

Figure 4a shows the adsorption efficiencies of Direct Red 80 (DR80) dye on different particle sizes of IFS powder. The one-way analysis of variance (ANOVA) and Tukey's test indicate that the particles retained on the 150 μm mesh have a DR80 removal efficiency of 45.33 ± 0.89%; this value is significantly higher ($p < 0.05$) than the removal efficiency of the particles retained on the 300, 425, and 600 μm meshes at 95% confidence. This is because the smaller the particle size, the greater the contact surface area with available sites for DR80 adsorption, since the smaller the particle size, the greater the specific surface area [42].

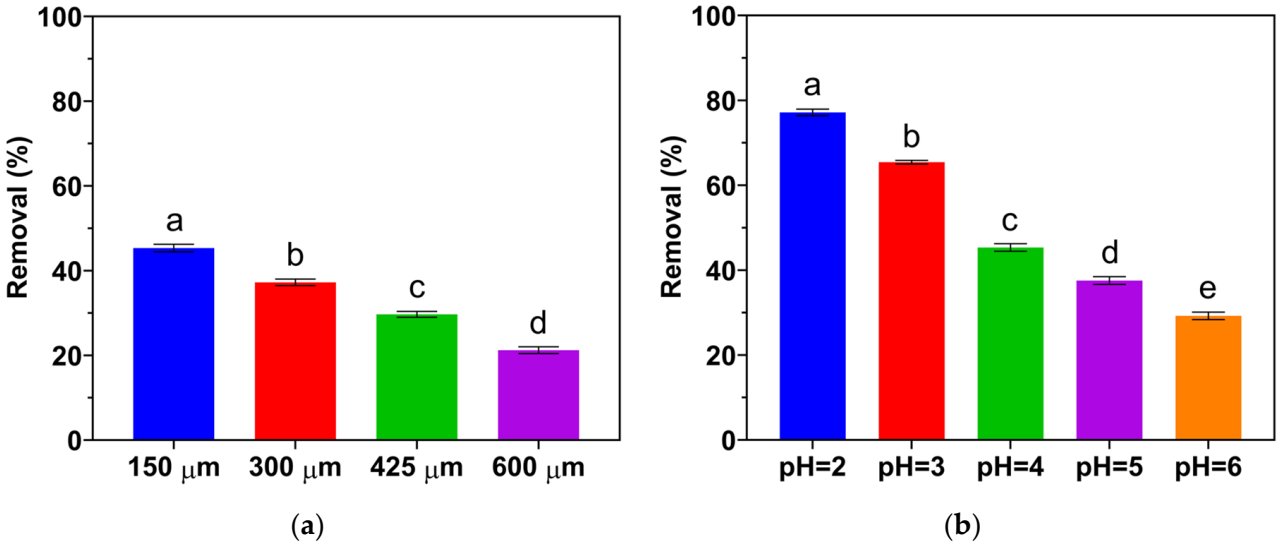


Figure 4. Adsorption efficiency (removal (%)) of Direct Red 80 at (**a**) different particle sizes of *Inga feuilleei* seed powder and at (**b**) different pH values of the aqueous medium. Different letters indicate a significant difference ($p < 0.05$).

3.4. pH Effect

Figure 4b shows the adsorption efficiencies at different pH values of the medium, with a removal efficiency of 77.15 ± 0.77% at pH = 2. One-way ANOVA and Tukey's post hoc test showed that at pH = 2, the removal efficiency was significantly higher ($p < 0.05$)

than the efficiencies found at pH values of 3, 4, 5, and 6. It is also observed that as the pH decreases, the removal efficiency increases. This would be because pH = 2, which is below the pH_{PZC} = 4.67, which confirms that the IFS surface would be positively charged, attracting DR80 electrostatically. This is confirmed by Pirillo et al. [43], who indicate that anions are favorably adsorbed at low pH due to the high H^+ concentration, which would explain the higher adsorption efficiency of the anionic dye DR80 at lower pH.

3.5. FTIR Characterization

Figure 5 presents the results of the ATR-FTIR analysis of the IFS powder before and after the DR80 adsorption process. In this figure, the red line spectrum corresponds to the natural IFS powder, which presents signals at 3273 cm^{-1}, corresponding to stretching vibrations of -OH groups. Also, peaks at 2927 and 2877 cm^{-1} are observed, C-H stretching vibrations corresponding to $-CH_2$ chains. At 1636 cm^{-1}, there are C=C stretching vibrations, and at 1379 cm^{-1}, it could correspond to deformation vibrations of C-H groups. At 994 and 859 cm^{-1}, a peak is observed that could correspond to the vibration of the C-C skeleton, and at 762 cm^{-1}, oscillating vibrations of CH_2 are present. On the other hand, Figure 5 shows the black line ATR-FTIR spectrum corresponding to the IFS powder after DR80 adsorption (IFS-DR80), where it can be noted that the intensity of the signals increased with respect to the IFS powder, so this increase in the vibrations would be due to the adsorption of DR80 on the IFS powder. Similar results were reported by the study of Sathya et al. [44] and Akhouairi et al. [45], who also found an increase in peak intensity after adsorption of Congo Red and Eriochrome Black T, respectively.

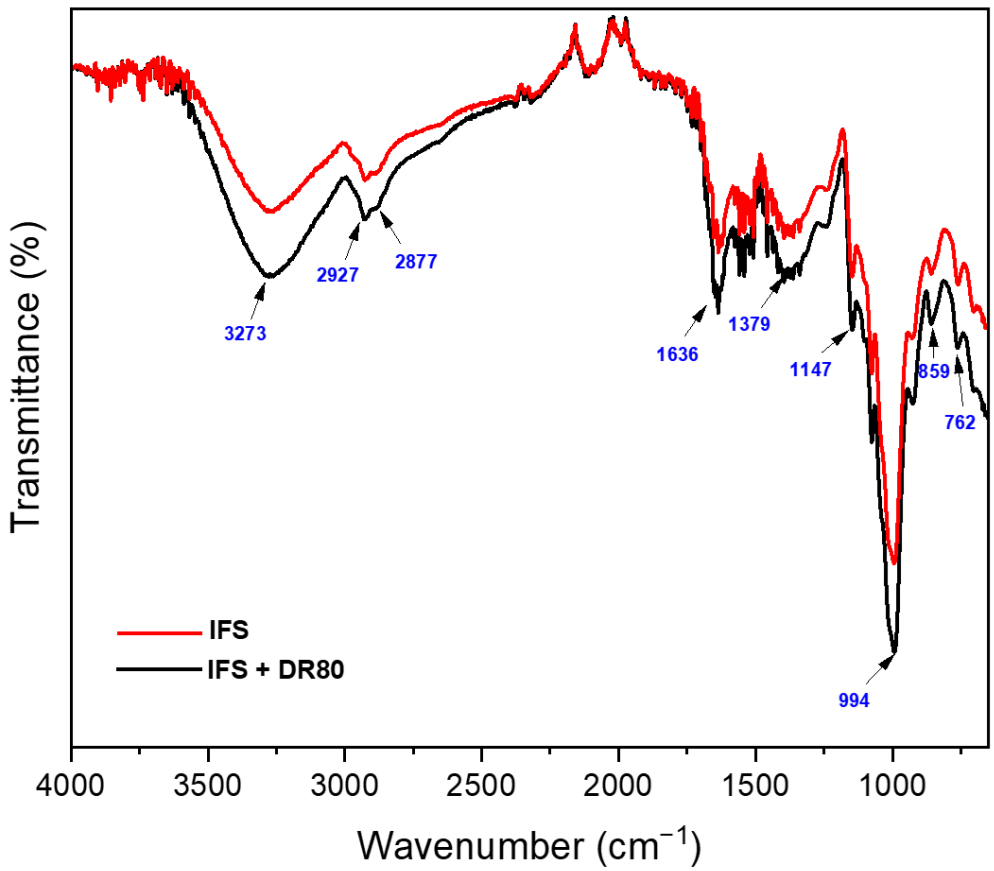


Figure 5. FTIR spectra of *Inga feuilleei* seeds (IFS, black line), and *Inga feuilleei* seed residues + Direct Red 80 (IFS + DR80).

3.6. Kinetic Study

Figure 6 shows the fit plot of the adsorption capacity "q_t" as a function of time to the pseudo-second-order kinetic model at 20, 30, 40, and 50 °C, considering initial DR80 concentrations of 100, 200, 300, and 400 mg/L.

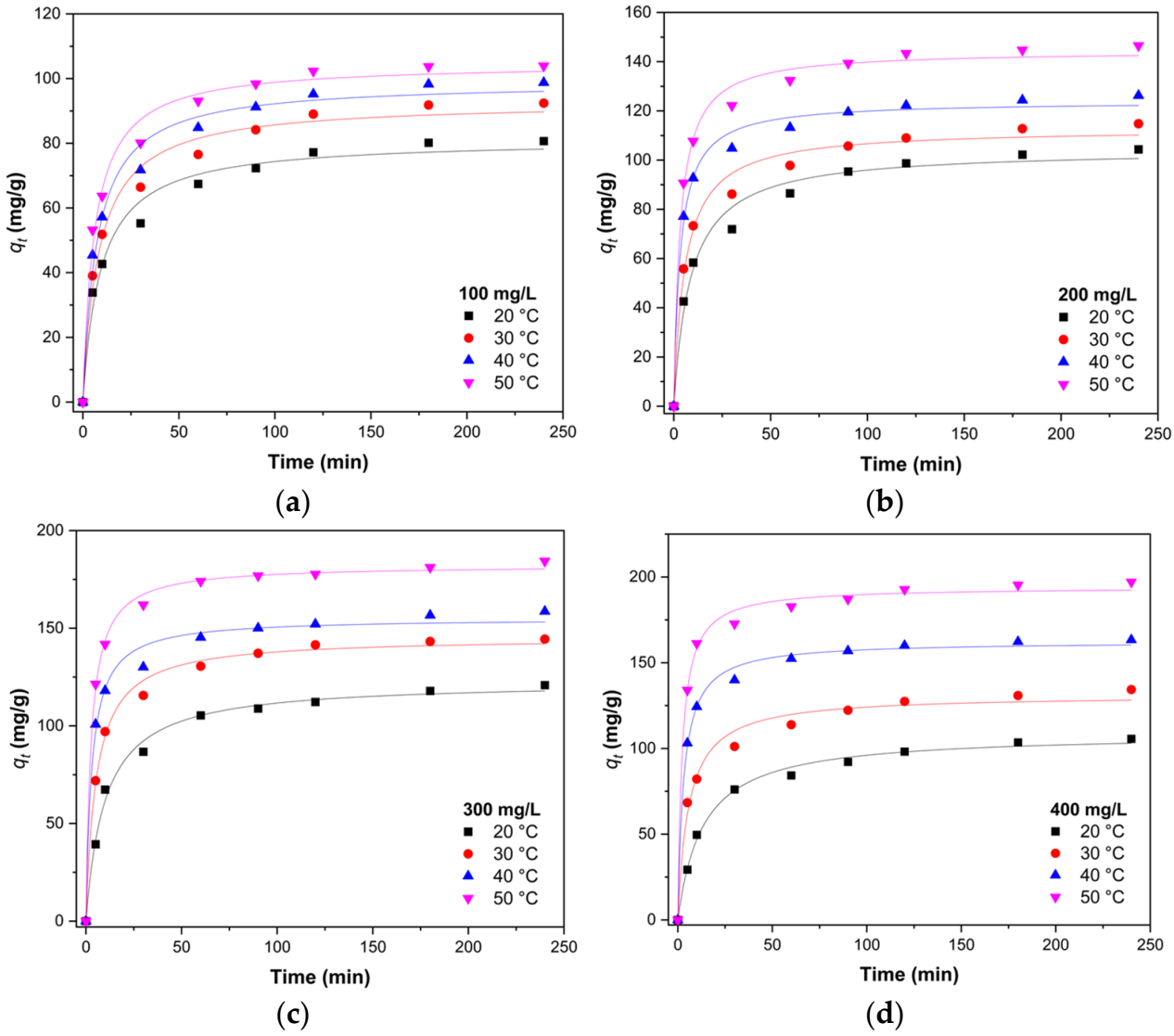


Figure 6. Pseudo-second-order kinetics at different temperatures of Direct Red 80 adsorption at concentrations of (**a**) 100 mg/L, (**b**) 200 mg/L, (**c**) 300 mg/L, and (**d**) 400 mg/L on *Inga feuilleei* seed powder.

Table 1 shows the removal efficiencies of DR80 for IFS dust at 240 min, across different initial concentrations and temperatures. It is observed that by increasing the initial concentration of DR80, the adsorption efficiency (removal (%)) decreases. It is also observed that the increase in temperature results in an increase in removal efficiency. On the other hand, it is observed that, in all cases, the pseudo-second-order kinetic model fits the experimental data better with a higher R^2 than the pseudo-first-order model. The fit to the pseudo-second-order model indicates that the main mechanism of adsorption is chemisorption [46].

Table 1. Adsorption efficiency and calculated parameters of the pseudo-first order and pseudo-second order for Direct Red 80 adsorption.

T (°C)	C_i (mg/L)	Removal %	q_{exp} (mg/g)	Pseudo-First Order			Pseudo-Second Order		
				k_1 (min^{-1})	q_e, cal (mg/g)	R^2	k_2 (g mg^{-1} min^{-1})	q_e, cal (mg/g)	R^2
20	100	77.55	80.68	0.0821	74.13	0.9279	0.0013	81.21	0.9796
	200	55.59	104.38	0.0882	95.37	0.9330	0.0011	104.29	0.9822
	300	41.86	120.84	0.0775	111.74	0.9652	0.0008	122.75	0.9932
	400	26.08	105.66	0.0606	117.22	0.9669	0.0007	108.71	0.9947
30	100	88.37	92.41	0.0919	85.05	0.9372	0.0013	92.82	0.9842
	200	61.14	114.81	0.1066	105.11	0.9438	0.0015	112.82	0.9847
	300	50.02	144.40	0.1309	136.14	0.9656	0.0013	145.25	0.9942
	400	33.15	130.88	0.1269	142.35	0.9379	0.0013	151.17	0.9825
40	100	94.44	98.76	0.1021	91.32	0.9370	0.0014	98.98	0.9839
	200	67.22	126.22	0.1838	118.17	0.9652	0.0024	123.91	0.9915
	300	54.95	158.62	0.1969	148.32	0.9619	0.0021	155.15	0.9894
	400	40.31	163.32	0.1921	155.45	0.9747	0.0020	162.38	0.9956
50	100	99.39	103.93	0.1192	97.67	0.9465	0.0016	104.73	0.9873
	200	78.05	146.56	0.1850	137.81	0.9645	0.0021	144.45	0.9915
	300	63.90	184.44	0.2064	175.37	0.9795	0.0021	182.34	0.9975
	400	48.64	195.38	0.2326	187.42	0.9815	0.0023	194.12	0.9951

3.7. Isotherms

Figure 7 presents the fit plots of the Langmuir and the Freundlich isotherm models at temperatures of 20, 30, 40, and 50 °C. All graphs show that the Langmuir model best fits the experimental data at all four temperatures studied.

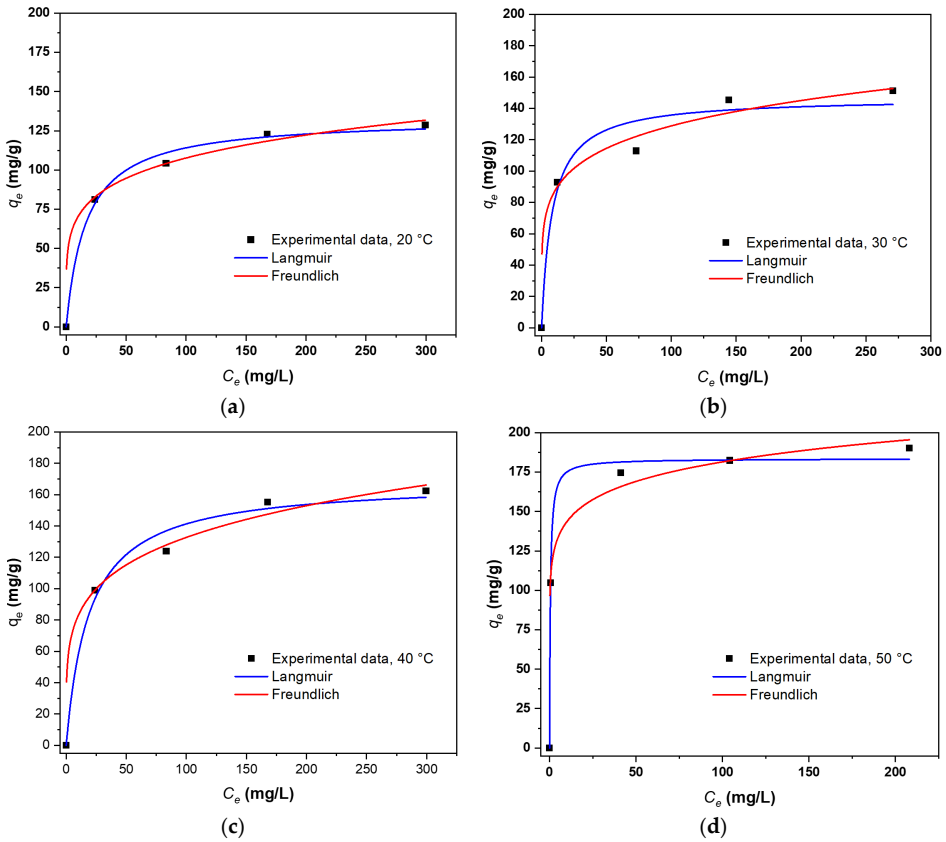


Figure 7. Adsorption isotherms of Direct Red 80 onto *Inga feuilleei* seed powder at temperatures of (**a**) 20 °C, (**b**) 30 °C, (**c**) 40 °C, and (**d**) 50 °C.

Table 2 shows the parameter values of the Langmuir and the Freundlich isotherm models. The Langmuir model was a better fit to the experimental data than the Freundlich model because the R^2 coefficient was closer to 1. According to the Langmuir model, the maximum adsorption capacity of DR80 on IFS powder increases with increasing temperature, being 133.11, 146.78, 152.78, and 183.51 mg/g at 20, 30, 40, and 50 °C, respectively. The Langmuir isotherm indicates that the adsorption of DR80 on IFS powder is uniform, and DR80 occupies the adsorption sites in a monolayer [47].

Table 2. Calculated parameters of Langmuir and Freundlich isotherms for Direct Red 80 adsorption.

Model	Parameters	Value			
		20 °C	**30 °C**	**40 °C**	**50 °C**
Langmuir	q_m (mg/g)	133.11	146.78	152.78	183.51
	K_L (L/mg)	0.0601	0.1229	0.2901	2.065
	R^2	0.9924	0.9544	0.9520	0.9862
Freundlich	$1/n$	0.1840	0.1703	0.1417	0.1019
	K_F	46.13	58.81	74.55	113.51
	R^2	0.9669	0.8931	0.9133	0.9466

Table 3 shows the comparison of the maximum adsorption capacity of DR80 obtained by IFS powder with other adsorbents studied at different experimental conditions, where it is noted that IFS presents a higher maximum adsorption capacity than Orange peel [48,49], Shells [50], and Potato peels [51], except Soy Meal Hull [52].

Table 3. Comparison of the maximum adsorption capacity of Direct Red 80 of different adsorbents with *Inga feuilleei* seed powder at different experimental conditions.

Adsorbent	T (K)	pH	C_0 (mg/L)	Adsorbent Dosage (g/L)	Stirring Time (min)/Stirring Speed (rpm)	Particle Size (μm)	q_{max} (mg/g)	Reference
Orange peel	298	2	50–125	4	25/200	--	21.05	[48,49]
Mixture shells	293	6	50–150	3.2	300/200	<106	28.50	[50]
External shells	293	6	50–150	3.2	300/200	<106	23.753	[50]
Internal shells	293	6	50–150	3.2	300/200	<106	22.00	[50]
Potato peels	303.16	2	100	20	60/100	100	27.778	[51]
Potato peels	313.16	2	100	20	60/100	100	45.45	[51]
Potato peels	323.16	2	100	20	60/100	100	32.258	[51]
Soy Meal Hull	293	2	50–150	0.3	120/200	<125	178.57	[52]
Inga feuilleei seed powder	293	2	100–400	1	240/350	150	133.11	This research
	303	2	100–400	1	240/350	150	146.78	This research
	313	2	100–400	1	240/350	150	152.78	This research
	323	2	100–400	1	240/350	150	183.51	This research

3.8. Thermodynamics

Figure 8 shows the Van't Hoff plot of $1/T$ versus $\ln K_c$, where the linear equation and the R^2 coefficient are observed. The intercept and slope of this linear equation were used to calculate the thermodynamic parameters.

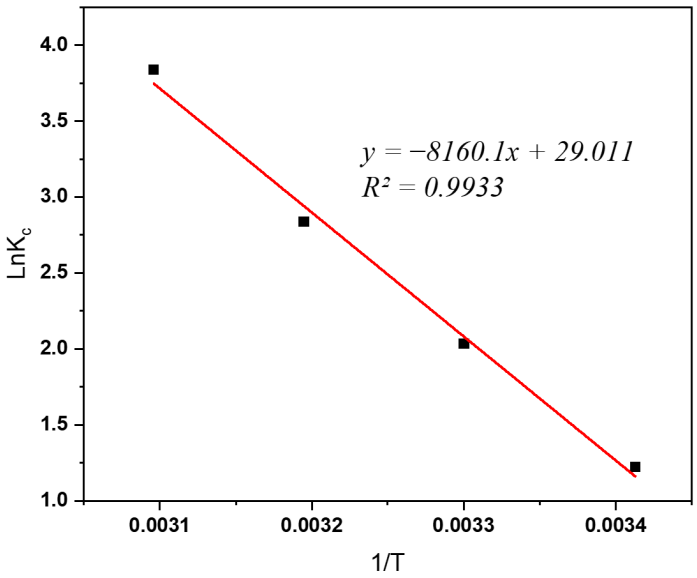


Figure 8. Van't Hoff plot of $1/T$ versus $\ln K_c$ for Direct Red 80 removal using *Inga feuilleei* powder as adsorbent at temperatures of 293, 303, 313, and 323 K.

Table 4 shows that the enthalpy value is 67.85 kJ/mol. The entropy value is 241.21 J/mol·K. The values of ΔG° become more negative as temperature increases, with the values at 293, 303, 313, and 323 K being −2.98, −5.12, −7.38, and 10.30 kJ/mol, respectively. When ΔG° is negative, the process is spontaneous, and when it becomes more negative with increasing temperature, it indicates that it is less favorable with increasing temperature [53].

Table 4. Thermodynamic parameters at different temperatures for Direct Red 80 adsorption on *Inga feuilleei* powder.

T (K)	ΔH° (kJ/mol)	ΔS° (J/mol·K)	ΔG° (kJ/mol)
293	67.85	241.21	−2.98
303			−5.12
313			−7.38
323			−10.30

The value of the Langmuir constant (KL) increased significantly with the increase in temperature from 20 to 50 °C, rising from 0.0601 to 2.065 L/mg (Table 2). This trend indicates an improvement in the affinity between DR80 and IFS at higher temperatures. This behavior is thermodynamically consistent with the positive value of enthalpy (ΔH° = 67.85 kJ/mol), confirming the endothermic nature of the process. Furthermore, the magnitude of ΔH° is greater than 40 kJ/mol, which suggests that the adsorption mechanism is governed by chemisorption. The increase in KL values correlates with the more spontaneous nature of the system at higher temperatures, as demonstrated by the increasingly negative values of Gibbs free energy (ΔG°).

3.9. Reuse

Figure 9 shows the removal efficiency results in the five reuse cycles of IFS powder for the removal of DR 80. In the first cycle, 78.41% of DR 80 (initial concentration: 100 mg/L) was removed. In the second, third, and fourth cycles, this was reduced to 72.72%, 66.57%, and 56.17%, respectively. Finally, in the fifth cycle, the removal efficiency was reduced to 50.98%.

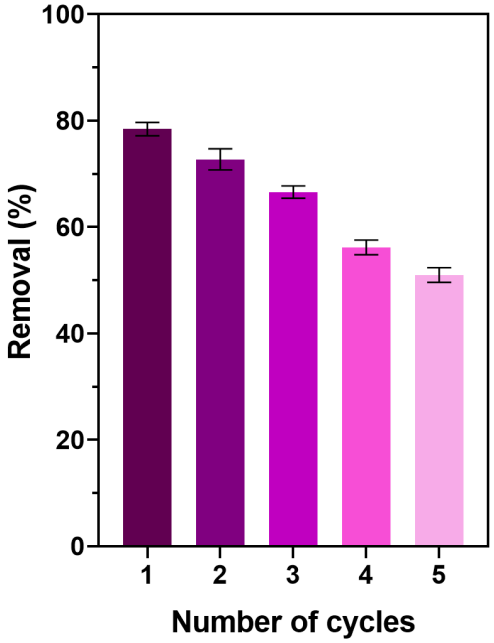


Figure 9. Adsorption efficiency (removal (%)) of Direct Red 80 with respect to adsorbent reuse cycles (IFS).

3.10. Techno-Economic Analysis

The techno-economic analysis for the calculation of *NPV*, *IRR*, *B/C*, and *IRP* of the project to produce IFS powder is presented in the Supplementary Material, and the results are presented in Table 5. The *NPV* was 35,701.46 USD. This result is positive, indicating that the production of this biomaterial will generate profits for the company, which confirms its viability. While in the *IRR*, a value of 25.47% was found, which is higher than "*COK* = 12.33% (Table S16)", this indicates that the project is profitable. In the case of "B/C", it was recorded with 1.49 USD, which is greater than 1, confirming the profitability of the project. For the IRP, a figure of 3.6289 was recorded, which, when broken down, shows that the return on investment period is 3 years, 7 months, and 16 days. In another adsorption study using grape seeds post-oil extraction, it was also found that the production of the adsorbent was feasible and cost-effective [37].

Table 5. Techno-economic analysis parameters.

Parameter	Value
NPV (USD)	35,701.46
IRR (%)	25.47
B/C	1.49
IRP	3.6289

4. Conclusions

Inga feuilleei seed (IFS) powder has a rough, irregular, heterogeneous, and porous morphology that would confer to this material adsorption properties of the Direct Red 80 (DR80) dye. The highest removal efficiency of IFS powder occurs at pH = 2 and IFS powder particle size of 150 µm. One of the mechanisms involved in the adsorption process of DR80 is electrostatic attraction because the highest removal efficiency occurred at pH below the point of zero charge (pH_{PZC} = 4.67). ART-FTIR analysis of the IFS powder showed the presence of -OH, C=C, and C-H groups. The pseudo-second-order kinetic model was a better fit to the experimental data of removal capacity, indicating that another limiting mechanism in the adsorption process is chemisorption. According to the Langmuir

isotherm model, the maximum adsorption capacity of DR80 on IFS powder is 133.11, 146.78, 152.78, and 183.51 mg/g at 20, 30, 40, and 50 °C, respectively, which shows that the adsorption capacity of IFS powder increases with temperature. The Gibbs energy change became more negative with increasing temperature, indicating that the adsorption process was endothermic and spontaneous. Finally, the use of IFS powder is a cost-effective alternative, since the approach of a project for the development of the production process of this adsorbent is viable with a positive *NPV*, and it is also profitable with an *IRR* greater than *COK*, *B/C* greater than 1, with an *IRP* of 3 years, 7 months, and 16 days.

Supplementary Materials: The following supporting information can be downloaded at: https://www.mdpi.com/article/10.3390/pr14060968/s1, Table S1: Tangible Fixed Assets; Table S2: Intangible fixed assets; Table S3: Production area; Table S4: Areas of the company; Table S5: Working Capital; Table S6: Raw material cost; Table S7: Labor cost; Table S8: Indirect manufacturing costs; Table S9: Machinery depreciation; Table S10: Administrative expenses; Table S11: Investment budget; Table S12: Debt budget or investor financing; Table S13: Loan amortization; Table S14: Production costs; Table S15: IFS Powder Cost; Table S16: Opportunity cost of capital "COK"; Table S17: Weighted average cost of capital (WACC); Table S18: Income statement; Table S19: Economic cash flow; Table S20: Financial Cash Flow. References [37,54–59] are cited in the Supplementary Materials.

Author Contributions: Conceptualization, E.G.G.-C., J.A.V.-S., and O.A.P.-C.; methodology, E.G.G.-C., M.L.S.-A., M.F.M.-C.; software, E.G.G.-C.; validation, E.G.G.-C., and J.G.-C.; formal analysis, E.G.G.-C., J.G.-C., and J.A.V.-S.; investigation, E.G.G.-C., M.L.S.-A., M.F.M.-C.; resources, E.G.G.-C., and O.A.P.-C.; data curation, E.G.G.-C. and J.G.-C.; writing—original draft preparation, E.G.G.-C., M.L.S.-A., and M.F.M.-C.; writing—review and editing, E.G.G.-C. and J.A.V.-S.; visualization, E.G.G.-C. and J.G.-C.; supervision, E.G.G.-C. and J.A.V.-S.; project administration, O.A.P.-C.; funding acquisition, O.A.P.-C. All authors have read and agreed to the published version of the manuscript.

Funding: This research was funded by the Technological University of Peru, under code I+D_SUR_2021_022.

Data Availability Statement: The original contributions presented in this study are included in the article/Supplementary Material. Further inquiries can be directed to the corresponding authors.

Conflicts of Interest: The authors declare no conflicts of interest. The funders had no role in the design of the study; in the collection, analyses, or interpretation of data; in the writing of the manuscript; or in the decision to publish the results.

Abbreviations

The following abbreviations are used in this manuscript:

IFS	*Inga feuilleei* seed
DR80	Direct Red 80
FTIR	Fourier Transform Infrared Spectroscopy
ATR	Attenuated Total Reflectance
pH_{PZC}	Point of zero charge
SEM	Scanning Electron Microscope
ANOVA	Analysis of variance
R^2	coefficient of determination
q_t	Adsorption capacity
m	Weight
V	Volume
Ci	Initial concentration
Cf	Final concentration

k_1	Pseudo-first order constant
k_2	Pseudo-second order
q_e	Adsorption capacity at equilibrium
t	Time
C_e	Concentration of DR80 at equilibrium
q_m	Maximum adsorption capacity
K_L	Langmuir constant
n	Freundlich constant
ΔS^0	Entropy
ΔH^0	Enthalpy
ΔG^0	Gibbs energy
T	Temperature
R	Universal gas constant
K_c	Equilibrium constant
NPV	Net Present Value
IRR	Internal Rate of Return
B/C	Benefit/cost
IRP	Investment Recovery Period
CF	Cash Flow
I_0	Initial investment
i	Discount rate
A	Immediate previous year of recovery
B	Initial investment
C	Accumulated cash flow
D	Economic cash
COK	Cost of Opportunity of Capital

References

1. Rathinam, A.; Jaiswal, R.; Chellam, P.V. Occurrence and Distribution of Emerging Contaminants: Ozonolytic Removal in Aqueous Matrices. In *Bioremediation of Emerging Contaminants in Water. Volume 1*; ACS Symposium Series; American Chemical Society: Washington, DC, USA, 2024; Volume 1475, pp. 111–127. [CrossRef]
2. Patel, D.; Jain, K.R.; Madamwar, D.; Desai, C. Phytotechnologies for Bioremediation of Textile Dye Wastewater. In *Phytoremediation for Environmental Sustainability*; Prasad, R., Ed.; Springer Nature: Singapore, 2021; pp. 251–272. [CrossRef]
3. Kaur, J.; Tewari, S.; Kaur, A.; Malik, R. Dye and Dye-Containing Hazardous Waste in Water Resource. In *Emerging Contaminants in Water and Wastewater: Sources and Substances*; Gupta, H., Madhav, S., Dhiman, S., Mishra, R., Eds.; Springer Nature: Cham, Switzerland, 2025; pp. 179–199. [CrossRef]
4. Lekhak, U.M. 2-Ecotoxicity of synthetic dyes. In *Current Developments in Bioengineering and Biotechnology*; Govindwar, S.P., Kurade, M.B., Jeon, B.-H., Pandey, A., Eds.; Elsevier: Amsterdam, The Netherlands, 2023; pp. 45–67. [CrossRef]
5. Chung, K.-T. Azo dyes and human health: A review. *J. Environ. Sci. Health Part C Environ. Carcinog. Ecotoxicol. Rev.* **2016**, *34*, 233–261. [CrossRef] [PubMed]
6. PubChem Direct Red 80. Available online: https://pubchem.ncbi.nlm.nih.gov/compound/Direct-Red-80 (accessed on 1 March 2026).
7. Song, Y.; Sun, K.; Liu, R. An exploration of the interaction mechanism of Direct Red 80 with α-Amylase at the molecular level. *J. Mol. Recognit.* **2021**, *34*, e2883. [CrossRef]
8. Kurade, M.B.; Jadhav, U.U.; Phugare, S.S.; Kalyani, D.C.; Govindwar, S.P. 1-Global scenario and technologies for the treatment of textile wastewater. In *Current Developments in Bioengineering and Biotechnology*; Govindwar, S.P., Kurade, M.B., Jeon, B.-H., Pandey, A., Eds.; Elsevier: Amsterdam, The Netherlands, 2023; pp. 1–43. [CrossRef]
9. Sridharan, R.; Krishnaswamy, V.G. Bioremediation of Textile Dyes for Sustainable Environment—A Review. In *Modern Approaches in Waste Bioremediation: Environmental Microbiology*; Shah, M.P., Ed.; Springer International Publishing: Cham, Switzerland, 2023; pp. 447–460. [CrossRef]
10. Ganguly, A.; Nanda, S.; Das, K.; Ghanty, S.; Biswas, G.; Mandi, M.; Mukherjee, S.; Paramanik, M.; Rajak, P. Micropollutants in Environment. In *Ecosystem Management*; John Wiley & Sons, Ltd.: Hoboken, NJ, USA, 2024; pp. 453–492. [CrossRef]

11. Yazdandoust, M.; Ehrampoush, M.H.; Dalvand, A. *Moringa oleifera* seed extract assisted electrocoagulation process for efficient direct dye removal from textile wastewater: Modelling, optimisation and techno-economic study. *Int. J. Environ. Anal. Chem.* **2024**, *104*, 2485–2505. [CrossRef]
12. Puiatti, G.A.; Elerate, E.M.; de Carvalho, J.P.; Luciano, V.A.; de Carvalho Teixeira, A.P.; Lopes, R.P.; Teixeira de Matos, A. Reuse of iron ore tailings as an efficient adsorbent to remove dyes from aqueous solution. *Environ. Technol.* **2024**, *45*, 2308–2319. [CrossRef]
13. Sadeghy, S.; Pormazar, S.M.; Ghaneian, M.T.; Ehrampoush, M.H.; Dalvand, A. Modeling and optimization of direct dyes removal from aqueous solutions using activated carbon produced from sesame shell waste. *Sci. Rep.* **2024**, *14*, 24867. [CrossRef]
14. Mazlan, N.A.; Lewis, A.; Chen, Z.; Butt, F.S.; Han, J.; Radacsi, N.; Yang, S.; Huang, Y. Photocatalytic self-cleaning graphene oxide/ZnO hybrid membrane for ultrafast cyclic small organic molecule separation. *J. Membr. Sci.* **2024**, *697*, 122539. [CrossRef]
15. Hamami, Z.; Javanbakht, V. Photocatalytic processes using potato peel extract-mediated CuO nanophotocatalyst for fast and efficient direct red 80 dye removal. *Biomass Convers. Biorefin.* **2025**, *15*, 563–573. [CrossRef]
16. do Carmo Dias, G.; de Souza, N.C.S.; de Souza, E.I.P.; Puiatti, G.A.; Moreira, R.P.L. Enhanced degradation of Direct Red 80 dye via Fenton-like process mediated by cobalt ferrite: Generated superoxide radicals and singlet oxygen. *Environ. Sci. Pollut. Res.* **2024**, *31*, 28025–28039. [CrossRef] [PubMed]
17. Kouzi, Y.; Chafiq Elidrissi, Z.; Achiou, B.; Beqqour, D.; Alami Younssi, S.; Rabiller-Baudry, M.; Bouhria, M.; Ouammou, M. Enhancing stability and performance of graphene oxide membrane grafted on low-cost rich-silica support: A comparative study of two activation approaches. *Process Saf. Environ. Prot.* **2024**, *188*, 1574–1583. [CrossRef]
18. Essate, A.; El Machtani Idrissi, D.; Achiou, B.; Adlane, S.; Breida, M.; Curcio, S.; Chakraborty, S.; Alami Younssi, S.; Ouammou, M. High-performance zeolite-A/polystyrene composite membrane tailored for efficient soluble dyes separation and antifouling. *Colloids Surf. Physicochem. Eng. Asp.* **2024**, *703*, 135162. [CrossRef]
19. Liu, J.; Qin, Z.; Yang, L.; Wei, J.; Feng, C.; Tang, B.; Jiang, W.; Yang, L.; Yao, L.; Zheng, J.; et al. Ultra-fast molecular sieving in ZIF-67 and cellulose nanofibers based thin-film nanocomposite membrane. *Sep. Purif. Technol.* **2025**, *355*, 129753. [CrossRef]
20. Yang, M.; Li, L.; Wu, X.; Tian, H. Preparation of covalent organic framework mixed matrix membranes and their application in liquid separation. *J. Environ. Chem. Eng.* **2025**, *13*, 118836. [CrossRef]
21. Adlane, S.; Essate, A.; Naim, J.; Achiou, B.; Tiraferri, A.; Aaddane, A.; Youssefi, S.; Ouammou, M.; Alami Younssi, S. Development and characterization of a purified pyrophyllite-based ultrafiltration membrane for the treatment of dye-contaminated water. *J. Environ. Chem. Eng.* **2025**, *13*, 118579. [CrossRef]
22. Kouzi, Y.; Chafiq Elidrissi, Z.; Essate, A.; Beqqour, D.; Achiou, B.; Alami Younssi, S.; Rabiller-Baudry, M.; Bouhria, M.; Ouammou, M. Tailored rGO-TiO2-pPD low-cost ceramic membrane for dye wastewater filtration: A synergistic strategy of GO reduction, intercalation and crosslinking. *Sep. Purif. Technol.* **2025**, *378*, 134643. [CrossRef]
23. Barman, F.; Nath, S.; Dey, S.; Ansari, M.T.A.; Kundu, R.; Paul, S. Aquatic Plant-Mediated Bioremediation Strategies. In *Toxicity of Aquatic System and Remediation*; CRC Press: Boca Raton, FL, USA, 2024. [CrossRef]
24. Alsharif, M.A. *Understanding Adsorption: Theories, Techniques, and Applications*; IntechOpen: London, UK, 2025. [CrossRef]
25. Akhtar, M.; Hasany, S.M.; Bhanger, M.I.; Iqbal, S. Low cost sorbents for the removal of methyl parathion pesticide from aqueous solutions. *Chemosphere* **2007**, *66*, 1829–1838. [CrossRef]
26. Mo, J.; Yang, Q.; Zhang, N.; Zhang, W.; Zheng, Y.; Zhang, Z. A review on agro-industrial waste (AIW) derived adsorbents for water and wastewater treatment. *J. Environ. Manag.* **2018**, *227*, 395–405. [CrossRef]
27. Prance, G.T. FRUITS OF TROPICAL CLIMATES | Fruits of Central and South America. In *Encyclopedia of Food Sciences and Nutrition (Second Edition)*; Caballero, B., Ed.; Academic Press: Oxford, UK, 2003; pp. 2810–2816. [CrossRef]
28. Lima, L.d.S.; Fernandes, E.P.; Novelli, A.; da Costa, L.P.; Monteiro, M.D.S.; dos Santos, M.V.Q.; Freitas, J.A.; Sussuchi, E.M. Adsorption and ecotoxicology studies with aqueous solution of Cr(VI) ions using adsorbent materials derived from *Inga edulis*. *Chemosphere* **2025**, *378*, 144378. [CrossRef]
29. Silva, E.M.; Pompeu, D.R.; Larondelle, Y.; Rogez, H. Optimisation of the adsorption of polyphenols from *Inga edulis* leaves on macroporous resins using an experimental design methodology. *Sep. Purif. Technol.* **2007**, *53*, 274–280. [CrossRef]
30. Georgin, J.; Franco, D.S.P.; Netto, M.S.; de Salomón, Y.L.O.; Piccilli, D.G.A.; Foletto, E.L.; Dotto, G.L. Adsorption and mass transfer studies of methylene blue onto comminuted seedpods from *Luehea divaricata* and *Inga laurina*. *Environ. Sci. Pollut. Res.* **2021**, *28*, 20854–20868. [CrossRef]
31. Franco, D.S.P.; Georgin, J.; Netto, M.S.; Fagundez, J.L.S.; Salau, N.P.G.; Allasia, D.; Dotto, G.L. Conversion of the forest species *Inga marginata* and *Tipuana tipu* wastes into biosorbents: Dye biosorption study from isotherm to mass transfer. *Environ. Technol. Innov.* **2021**, *22*, 101521. [CrossRef]
32. Correia, L.P.; Peron, A.P.; Sia, N.B.P.; Medeiros, F.V.d.S. Evaluation of *Macrolobium acaccifolium* and *Inga nobilis* Seeds in Coagulation/flocculation Processes. *Chem. Eng. Trans.* **2022**, *92*, 1–6. [CrossRef]
33. Brennan, E.B.; Mudge, K.W. Vegetative propagation of *Inga feuillei* from shoot cuttings and air layering. *New For.* **1998**, *15*, 37–51. [CrossRef]

34. Lim, T.K. *Inga feuillei* . In *Edible Medicinal and Non-Medicinal Plants: Volume 2, Fruits*; Lim, T.K., Ed.; Springer: Dordrecht, The Netherlands, 2012; pp. 720–722. [CrossRef]
35. Choquenaira-Quispe, C.; Villanueva-Salas, J.A.; Yucra-Condori, H.R.; Angulo Vargas, S.J.; Rojas Tamata, K.; Gonzales-Condori, E.G. "Chacco" clay from the Peruvian highlands as a potential adsorbent of heavy metals in water. *Energy Nexus* **2024**, *16*, 100330. [CrossRef]
36. Gonzales-Condori, E.G.; Avalos-López, G.; Gonzales-Condori, J.; Mujica-Guzmán, A.; Terán-Hilares, R.; Briceño, G.; Quispe-Avilés, J.M.; Parra-Ocampo, P.J.; Villanueva-Salas, J.A. Universidad Tecnológica del Perú Avocado seed powder residues as a promising bio-adsorbent for color removal from textile wastewater. *Rev. Mex. Ing. Quím.* **2023**, *22*, 1–23. [CrossRef]
37. Gonzales-Condori, E.G.; Bejar-Aramburu, D.G.; Gutierrez-Delgado, J.A.; Villanueva-Salas, J.A.; Gonzales-Condori, J.; Salazar-Pinto, B.M. Valorization of grape seed residues post-oil extraction as an adsorbent for hexavalent chromium in water. Kinetics, isotherms, thermodynamics, and techno-economic analysis. *Energy Nexus* **2025**, *18*, 100437. [CrossRef]
38. Inyinbor, A.A.; Adekola, F.A.; Olatunji, G.A. Copper scavenging efficiency of adsorbents prepared from *Raphia hookeri* fruit waste. *Sustain. Chem. Pharm.* **2019**, *12*, 100141. [CrossRef]
39. Macedo, M.C.C.; Correia, V.T.d.V.; Silva, V.D.M.; Pereira, D.T.V.; Augusti, R.; Melo, J.O.F.; Pires, C.V.; de Paula, A.C.C.F.F.; Fante, C.A. Development and Characterization of Yellow Passion Fruit Peel Flour (*Passiflora edulis* f. flavicarpa). *Metabolites* **2023**, *13*, 684. [CrossRef] [PubMed]
40. Montalvo Andia, J.; Larrea, A.; Salcedo, J.; Reyes, J.; Lopez, L.; Yokoyama, L. Synthesis and characterization of chemically activated carbon from *Passiflora ligularis*, *Inga feuilleei* and native plants of South America. *J. Environ. Chem. Eng.* **2020**, *8*, 103892. [CrossRef]
41. Ait Haki, M.; Imgharn, A.; Aarab, N.; Hsini, A.; Essekri, A.; Laabd, M.; El Jazouli, H.; Elamine, M.; Lakhmiri, R.; Albourine, A. Efficient removal of crystal violet dye from aqueous solutions using sodium hydroxide-modified avocado shells: Kinetics and isotherms modeling. *Water Sci. Technol.* **2021**, *85*, 433–448. [CrossRef]
42. Liu, Y.; Miao, J.; Han, H.; Xu, P. Differences in Influence of Particle Size on the Adsorption Capacity between Deformed and Undeformed Coal. *ACS Omega* **2021**, *6*, 5886–5897. [CrossRef] [PubMed]
43. Pirillo, S.; Ferreira, M.L.; Rueda, E.H. The effect of pH in the adsorption of Alizarin and Eriochrome Blue Black R onto iron oxides. *J. Hazard. Mater.* **2009**, *168*, 168–178. [CrossRef] [PubMed]
44. Sathya, K.; Jayalakshmi, H.; Reddy, S.N.; Ratnam, M.V.; Bandhu, D. Effective removal of Congo red dye using adsorbent prepared from bio-waste: Isotherm, kinetic, and thermodynamic studies. *Biomass Convers. Biorefin.* **2025**, *15*, 3557–3569. [CrossRef]
45. Akhouairi, S.; Ouachtak, H.; Addi, A.A.; Jada, A.; Douch, J. Natural Sawdust as Adsorbent for the Eriochrome Black T Dye Removal from Aqueous Solution. *Water Air Soil Pollut.* **2019**, *230*, 181. [CrossRef]
46. Reddy, Y.S.; Jose, T.J.; Dinesh, B.; Kumar, R.N.; Kumar, P.S.; Kaviyarasu, K. Equilibrium, kinetic, and thermodynamic study of Direct Yellow 12 dye adsorption by biomass-derived porous graphitic activated carbon. *Biomass Convers. Biorefin.* **2025**, *15*, 6817–6833. [CrossRef]
47. Serban, G.V.; Iancu, V.I.; Dinu, C.; Tenea, A.; Vasilache, N.; Cristea, I.; Niculescu, M.; Ionescu, I.; Chiriac, F.L. Removal Efficiency and Adsorption Kinetics of Methyl Orange from Wastewater by Commercial Activated Carbon. *Sustainability* **2023**, *15*, 12939. [CrossRef]
48. Arami, M.; Limaee, N.Y.; Mahmoodi, N.M.; Tabrizi, N.S. Removal of dyes from colored textile wastewater by orange peel adsorbent: Equilibrium and kinetic studies. *J. Colloid Interface Sci.* **2005**, *288*, 371–376. [CrossRef] [PubMed]
49. Doulati Ardejani, F.; Badii, K.; Yousefi Limaee, N.; Mahmoodi, N.M.; Arami, M.; Shafaei, S.Z.; Mirhabibi, A.R. Numerical modelling and laboratory studies on the removal of Direct Red 23 and Direct Red 80 dyes from textile effluents using orange peel, a low-cost adsorbent. *Dye. Pigment.* **2007**, *73*, 178–185. [CrossRef]
50. Doulati Ardejani, F.; Badii, K.; Limaee, N.Y.; Shafaei, S.Z.; Mirhabibi, A.R. Adsorption of Direct Red 80 dye from aqueous solution onto almond shells: Effect of pH, initial concentration and shell type. *J. Hazard. Mater.* **2008**, *151*, 730–737. [CrossRef]
51. Ben Jeddou, K.; Bouaziz, F.; Ben Taheur, F.; Nouri-Ellouz, O.; Ellouz-Ghorbel, R.; Ellouz-Chaabouni, S. Adsorptive removal of direct red 80 and methylene blue from aqueous solution by potato peels: A comparison of anionic and cationic dyes. *Water Sci. Technol.* **2021**, *83*, 1384–1398. [CrossRef]
52. Arami, M.; Limaee, N.Y.; Mahmoodi, N.M.; Tabrizi, N.S. Equilibrium and kinetics studies for the adsorption of direct and acid dyes from aqueous solution by soy meal hull. *J. Hazard. Mater.* **2006**, *135*, 171–179. [CrossRef]
53. Aljeboree, A.M.; Alshirifi, A.N.; Alkaim, A.F. Kinetics and equilibrium study for the adsorption of textile dyes on coconut shell activated carbon. *Arab. J. Chem.* **2017**, *10*, S3381–S3393. [CrossRef]
54. Matemáticas Financieras y Valoración-Google Books. Available online: https://www.google.com.pe/books/edition/Matem%C3%A1ticas_financieras_y_valoraci%C3%B3n/jCF1EAAAQBAJ?hl=es-419&gbpv=0 (accessed on 28 February 2026).
55. cajaarequipa.pe Tarifario de Tasas de Interés Activas. Caja Arequipa. Available online: https://www.cajaarequipa.pe/tasas-de-interes/tarifario-de-tasas-de-interes-activas/ (accessed on 28 February 2026).

56. Magueyal Salas, J.L. *Análisis y Reflexiones Sobre los Costos de Producción y Ventas*; Editorial Digital del Tecnológico de Monterrey: Monterrey, Mexico, 2020.
57. Fernández Espinoza, S. *Los Proyectos de Inversión: Evaluación Financiera*; Editorial Tecnologica de Costa Rica: Cartago, Costa Rica, 2007.
58. Guzman Castro, F. *El Estudio Económico-Financiero y la Evaluación en Proyectos de la Industria Química*; Universidad Nacional de Colombia: Bogota, Colombia, 2001.
59. Torrents, A.S.; Vilda, F.G.; Postils, I.A.; Postils, I.A. *Manual Práctico de Diseño de Sistemas Productivos*; Ediciones Díaz de Santos: Madrid, Spain, 2004.

Disclaimer/Publisher's Note: The statements, opinions and data contained in all publications are solely those of the individual author(s) and contributor(s) and not of MDPI and/or the editor(s). MDPI and/or the editor(s) disclaim responsibility for any injury to people or property resulting from any ideas, methods, instructions or products referred to in the content.